Thermochimica Acta 505 (2010) 1–13

Contents lists available at ScienceDirect

Thermochimica Acta

journal homepage: www.elsevier.com/locate/tca

Fast scanning power compensated differential scanning nano-calorimeter: 1. The device

E. Zhuravlev, C. Schick*

University of Rostock, Institute of Physics, Wismarsche Str. 43-45, 18051 Rostock, Germany

ARTICLE INFO

Article history:
Received 18 January 2010
Received in revised form 18 March 2010
Accepted 22 March 2010
Available online 30 March 2010

Keywords:
Fast scanning nano-calorimetry
Differential power compensation
Temperature calibration
Crystallization
Metals

ABSTRACT

Fast scanning calorimetry becomes more and more important because an increasing number of materials are created or used far from thermodynamic equilibrium. Fast scanning, especially on cooling, allows for the in situ investigation of structure formation, which is of particular interest in a wide range of materials like polymers, metals, and pharmaceuticals to name a few. Freestanding silicon nitride membranes are commonly used as low addenda heat capacity fast scanning calorimetric sensors. A differential setup based on commercially available sensors is described. To enhance performance of the device a new asymmetric power compensation scheme was developed. The hardware realization of the scheme and calculation of differential power are presented in the first part of this paper. The fast analog amplifiers allow calorimetric measurements up to 100,000 K/s. The lower limit is defined by the sensitivity of the device and is 1 K/s for sharp melting or crystallization events in metals and ca. 100 K/s for broad transitions in polymers. Another limiting factor is accuracy of sample temperature measurement. A strong dependency of temperature on sample placement on the sensor is observed; even reproducibility is within ±1 K. For finite sample thicknesses the commonly observed thermal lag must be considered too. Uncertainty of the temperature measurement based on previous thermopile calibration is in the order of ±10 K. A significant improvement is possible by adding a small particle of a temperature calibration standard, e.g. indium or tin, on top of the sample under investigation. Then uncertainty is about ±3 K. The second part of the paper describes sample heat capacity determination and an example to demonstrate the performance of the device.

1. Introduction—fast scanning calorimetric techniques

Conventional differential scanning calorimetry (DSC) is one of the few techniques that have a relatively large dynamic range of scanning rates. It allows (quasi) isothermal measurements and scanning rates up to 10 K/s for power compensated DSCs [1,2]. Several approaches are known how to increase scanning rate. Most of them are based on thin film techniques. Quasi-adiabatic scanning calorimetry at high heating rates, ca. 500 K/s, was developed by Hager [3] and even for rates up to 10^7 K/s, by Allen et al. [4,5]. Similar approaches were used to study the behavior of metastable materials like vapor deposited films [6–8]. But investigation of metastable phase formation is possible only if the same high controlled cooling rates are available too. Fastest cooling of a calorimetric cell is obtained if no heat is applied to the cell (electrical power $P_0(T) = 0$ in the heat balance Eq. (1.1)). The maximum possible cooling rate is therefore defined by the ratio between the heat flow rate away from the measuring cell ($P_{loss}(T)$) and the heat capacities of measuring cell (addenda) ($C_0(T)$) and sample ($C(T)$).

$$(C_0(T) + C(T))\frac{dT}{dt} = P_0(T) - P_{\text{loss}}(T) \tag{1.1}$$

At a given temperature $P_{loss}(T)$ is in first approximation, assuming conductive and convection losses only, proportional to the temperature difference to the heat sink. Linear cooling is realized by keeping the right hand side of Eq. (1.1) at a constant negative value by controlling heater power $P_0(T)$. This idea was realized for fast scanning non-adiabatic nano-calorimeters based on thin film sensors (Fig. 1) [9] with extremely small addenda and sample heat capacity. It was shown that a gas is the optimum cooling agent to achieve largest cooling rates [10–12]. Furthermore, thermopiles are better suited compared to resistive thermometers because they do not need an electrical current, which always generates some unwanted power. The technique described in [9,11] is based on a single thin film chip sensor and is capable of applying both controlled heating and controlled cooling at rates up to 10^6 K/s.

This single sensor ultra-fast scanning device [11] was successfully applied for the investigation of polymer melting and crystallization. The reorganization kinetics in PET and iPS was studied in combination with conventional DSC at scanning rates

* Corresponding author. Tel.: +49 381 498 6880; fax: +49 381 498 6882.
E-mail address: christoph.schick@uni-rostock.de (C. Schick).

0040-6031/$ – see front matter © 2010 Elsevier B.V. All rights reserved.
doi:10.1016/j.tca.2010.03.019

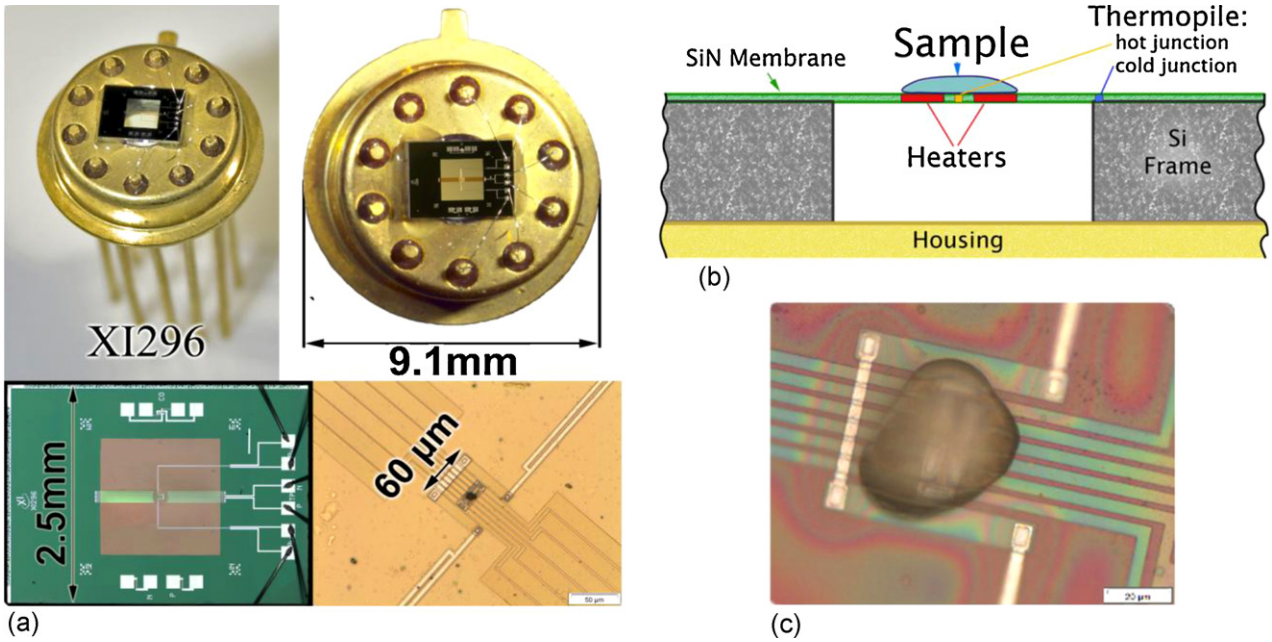

Fig. 1. Thin film chip sensor based on a thin free standing SiN_x film on a silicon frame and measuring area of 60 μm × 80 μm in the center of the film. (a) Different photographs of the sensor. (b) Schematic cross-section of the sensor with sample (not to scale). (c) Photomicrograph of a sample loaded sensor XI-296 [13].

covering 8 orders of magnitude [14–16]. Isothermal and non-isothermal crystallization and the formation of different crystal polymorphs were studied in a wide range of temperatures and scanning rates applying DSC and the fast scanning setup in PE, iPP and PVDF [9,17–24]. The complex behavior in the temperature range between glass transition and melting temperature was investigated in PBT [25]. The crystallization and cold crystallization suppression in PA6 confined to droplets and in the bulk was studied using such fast scanning calorimeter [26]. The dynamic range of scanning rates of the device allowed the investigation of superheating in linear polymers like iPS, PET, PBT and iPP [12,27].

The examples given above have shown that the effective range of controlled heating and cooling rates using different sensors [13] is 100–10^6 K/s. Unfortunately, at low rates signal to noise ratio and therefore sensitivity is reduced. Usually the device is limited to rates above 100 K/s for polymers. Nevertheless, the scanning rate range between conventional DSC and this technique – the range 10–100 K/s – is of high interest because several material processing steps are applying cooling rates just in this range [28,29].

In order to improve fast scanning nano-calorimetry the very successfully applied single sensor device as described in [9–11,30,31] was therefore first analyzed and the week points were identified.

- The first problem is the non-interactive temperature control, which is based on a predefined voltage–time profile yielding an essentially linear temperature increase of the sensor. But the needed voltage is only known for the empty sensor and not for the sample loaded one. Therefore the voltage profile should be corrected for each experiment by making at least one test scan with the sample under investigation [9]. This excludes the application to “first scans”, which are often needed if the influence of the sample history is of particular interest.
- Another problem is the sample temperature discontinuity at phase transitions. Even if a preliminary scan was performed to adjust the voltage profile for linear heating and cooling, the scanning rate during sharp transitions may significantly deviate from the programmed value due to large heat absorption or release by the sample. This results in smearing and inaccuracy of heat capacity and enthalpy determination. Similar problems exist for the adiabatic fast scanning devices [32].
- The main problem for heat capacity determination for the non-adiabatic single sensor device is the subtraction of the heat loss function. It is realized as a subtraction of a 3rd to 5th order polynomial function [9] providing C_p values symmetric around zero. But as soon as we have several sharp events in the sample, the error in determination of the loss polynomial increases dramatically. A solution to this problem is given in the second part of this paper [33].

To overcome these problems a differential scheme of two such sensors [9,11,34] with power compensation was constructed. The presence of an empty reference sensor reduces the influence of heat losses and addenda heat capacity on the obtained data dramatically. For a better sample temperature control, particularly in the transition regions, power compensation was introduced, this way following the work by Rodríguez-Viejo and co-workers [35,36] and Merzlyakov [37]. To improve signal to noise ratio and resolution of the device even under fast scanning conditions an analog power compensation technique was implemented. A differential power compensation scheme provides, under conditions of ideal symmetry of both sensors, directly the heat flow rate into the sample, which simplifies heat capacity calculation. Furthermore, user-friendly experiment management software and a software package for data evaluation were developed. The device including control and data treatment algorithms and measurements of metal samples on melting and solidification are presented finally to demonstrate the benefits of the instrument.

2. The device

The developed instrument is intended to measure heat flow rate into the sample as the power difference between an empty and a sample loaded sensor during fast temperature scans on heating and cooling at controlled rate. Finally, the obtained heat flow rate should be recalculated into heat capacity [33].

A very successful version of a power compensation differential scanning calorimeter was realized by PerkinElmer [38–41]. It

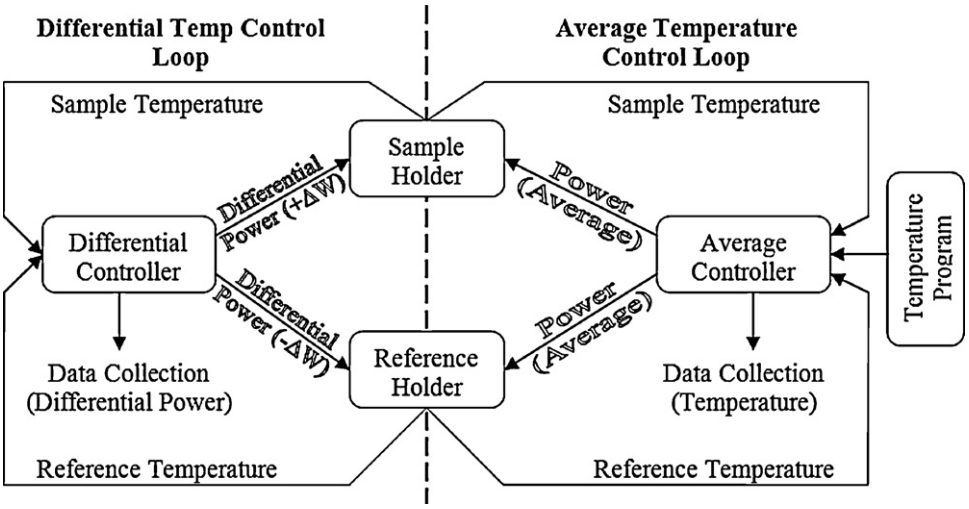

Fig. 2. PerkinElmer power compensation scheme: the average temperature controller makes both sensors to follow programmed temperature. The differential controller compensates the heat flow due to events in the sample and asymmetries. Symmetric compensation on reference and sample side simplifies computation of heat flow to the sample which was critical for that time when computers were not yet available [38–41].

is based on the measurement of the energy difference required to keep both sides, sample and reference, at the same temperature throughout the analysis. When an endothermic transition occurs, the energy absorbed by the sample is compensated by an increased energy input to the sample side to maintain the temperature balance. Because this energy input, under the assumption of a perfectly symmetric measuring system, is precisely equivalent in magnitude to the energy absorbed in the transition, a recording of this balancing energy yields a direct calorimetric measurement of the energy of the transition. The block diagram of the PerkinElmer power compensation DSC is shown in Fig. 2. It consists of two separate control loops: one for the control of the average temperature of both cups, the second for the control of the temperature difference between the cups.

The average controller compares the arithmetic average of sample and reference temperature with the program temperature. In case of a deviation the average controller corrects the electrical power to both cups accordingly. Due to the feedback the difference between measured average temperature and program temperature is minimized.

The second controller measures the temperature difference between both cups. Signals representing the sample and reference temperatures, measured by the platinum thermometers, are fed to the differential temperature amplifier. The differential temperature amplifier output will then adjust the power difference fed to the reference and sample heaters in the direction and magnitude necessary to correct any temperature difference between them. In case of a lower temperature of the sample cup, e.g. due to an endothermic transition, an additional power is added to the sample cup. In order to minimize the difference most effectively and to keep a strict symmetry of the measuring system the same power is subtracted on the reference side. Consequently, the heat of transition is not provided by the differential controller but by the average controller keeping the average temperature following the program temperature. The remaining temperature difference between both cups, which is proportional to the power difference [38–41], is recorded and together with the average temperature profile it provides the complete information about the heat flow rate to the sample. This scheme proves itself in PerkinElmer DSC calorimeters working up to 10 K/s scanning rate with milligram samples. Summarizing, in the PE differential power compensation DSC the additional heat needed (or released) during an endothermic (exothermic) event in the sample is finally provided by the average controller because the differential controller does not add or remove heat from the system due to its symmetric operation. This scheme allows for a relatively simple determination of the heat flow difference from the remaining temperature difference between sample and reference cups [38,40], not requiring measuring multiple signals or computing capabilities. But in this case both controllers must be fast to avoid deviations from the programmed temperature. Therefore it is common practice to use proportional controllers for average as well as differential loop.

But as soon as we wanted to go to higher rates and sensitivity we met the problem of controller performance limitations because the differential signal can contain fast events from the nanogram samples, requiring fast response of the controllers. Time resolution for the control of the average temperature could be much slower if the fast sample events would not be included. Output power range (dynamics) of the average controller is orders of magnitude larger than needed for the compensation of the sample related effects. Therefore it may be beneficial to separate average and difference control totally avoiding any cross-talk between both control loops.

Following this idea we developed a new power compensation scheme to realize such separate control loops as shown in Fig. 3 [42]. First, we measure and control reference sensors' temperature alone. No average temperature is used. There is no influence of any, even very strong, events occurring in the sample sensor on the reference temperature controller. This allows us to use a relatively slow but precise PID controller for the reference temperature control. The integral part of the controller assures that the difference between program temperature and reference temperature is practically zero. Applying the output voltage of the PID also to the sample sensor heater yields nearly the same temperature profile in the sample sensor as in the reference sensor if a high symmetry between reference and sample sensor is realized. Next, the differential controller detects any difference between reference and sample sensor temperatures and adds or subtracts its output voltage to the PID output voltage to the sample sensor alone. This way a total separation between both controllers is realized. It allows us to use a precisely but relatively slow working PID controller for the control of the reference temperature and a high sensitive and fast proportional controller for the difference controller.

Compared to the PerkinElmer power compensation scheme this allows a more precise control of the temperature of both sensors. But the proportionality between the remaining temperature difference in the differential control loop and the differential heat flow

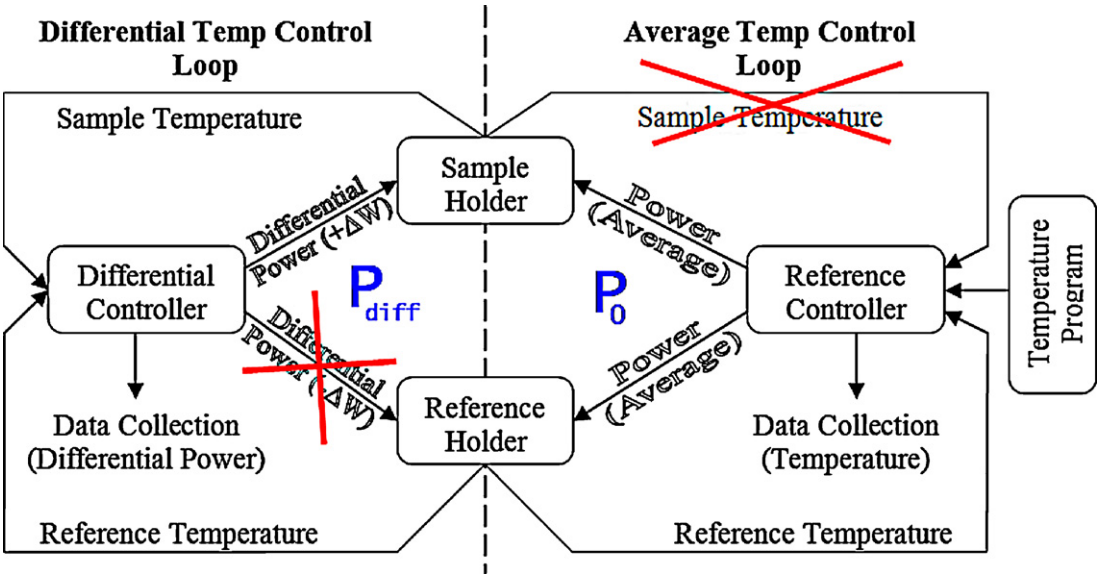

Fig. 3. Modified power compensation scheme for operation at high scanning rates: separation of average temperature control (slow changes, large dynamic range) and differential control (fast events, small dynamic range).

rate is lost. Therefore the new scheme requires the measurement of more than only one signal to allow recalculation of the power difference as it is described below.

The user defined experimental time–temperature profile is recalculated into voltage and provided as the setpoint for the PID controller. The PID controller makes the temperature of the reference sensor to follow the experimental profile by adjusting power P_0 to its heater. The same power P_0 is applied to the sample loaded sensor. The difference between the temperatures of reference and sample side is minimized by the differential controller by adding power P_{diff} to the sample side.

The resistive film-heaters of the sensors, ca. 1 kΩ, provide the power, which is supplied to the membrane/sample interface and propagates through the sample, membrane and the ambient gas. For a perfectly working power compensated system power is distributed in a way that both sensors are always at the same temperature, T, and scanned at the programmed rate, dT/dt, independent on any heat effect in the sample. Assuming such an ideally symmetric differential system means equal addenda heat capacities C_0 on both sides and equal heat losses $P_{loss}(T)$ to the surrounding on both sides. Then the heat balance equations for both sensors are as follows:

reference:

$$C_0(T)\frac{dT}{dt} = P_0(T) - P_{loss}(T) \tag{1.2}$$

sample:

$$(C_0(T) + C(T))\frac{dT}{dt} = P_0(T) + P_{diff}(T) - P_{loss}(T) \tag{1.3}$$

where C is sample heat capacity. In this particular case the difference between Eq. (1.2) and (1.3) yields

$$C(T)\frac{dT}{dt} = P_{diff}(T) \tag{1.4}$$

where P_{diff} is the difference between the power supplied to the sample and the reference sensor. Consequently, the aim was to setup a system with near to perfect power compensation, which allows determination of $P_{diff}(T)$ and finally to correct for unavoidable asymmetries between both sides in real measurements at high scanning rates.

The hardware was designed for that aim having in mind anticipated scanning rates of up to 100,000 K/s. The differential controller, see Fig. 4 below, was therefore realized as proportional controller to make it as fast as possible. Amplifiers with adjustable gain settings (X2 and X4[1]) were used for that purpose. The gain is always set to the maximum value, which still damps self-oscillations in the circuit. Analog electronics was used in the scheme to shorten response time and therefore allow high rate temperature processing. Power difference and all voltages needed for calculation are collected by the computer using a fast ADC/DAC board from Meilhaus [43]. A SRS Small Instrumentation Module analog device frame [44] allows controlling almost all parameters of the amplifiers from the computer. The program for managing the experiment and data collection is written in LabView™ graphical programming language version 8.6.

The separation of the two control loops makes recalculation of sample heat capacity more difficult in comparison to the symmetric power compensation scheme as it is used in the PerkinElmer power compensation DSC, but allows going to higher rates with reliable average temperature control as shown below. Deduction of heat capacity out of the measured signals consists of several steps. First is the determination of heat flow rate into the sample.

3. Electric scheme and power difference determination

The principal electric scheme of the device and the collected signals needed for power difference determination are shown in Fig. 4.

The power difference which we want to know is as follows:

$$P_{diff}(T) = \frac{(U^h_{sample})^2}{R^h_{sample}} - \frac{(U^h_{ref})^2}{R^h_{ref}} \tag{1.5}$$

where U^h_{sample} and U^h_{ref} are the voltage drops across sample and reference side heaters and R^h_{sample} and R^h_{ref} are their resistances, respectively. To avoid overloading the equations we do not indicate the temperature dependence of the quantities used in Eqs. (1.5)–(1.11), except the final result $P_{diff}(T)$. From the single sensor

[1] In the following X1, X2, X3, X4 and PID refer to the particular amplifiers in Fig. 4.

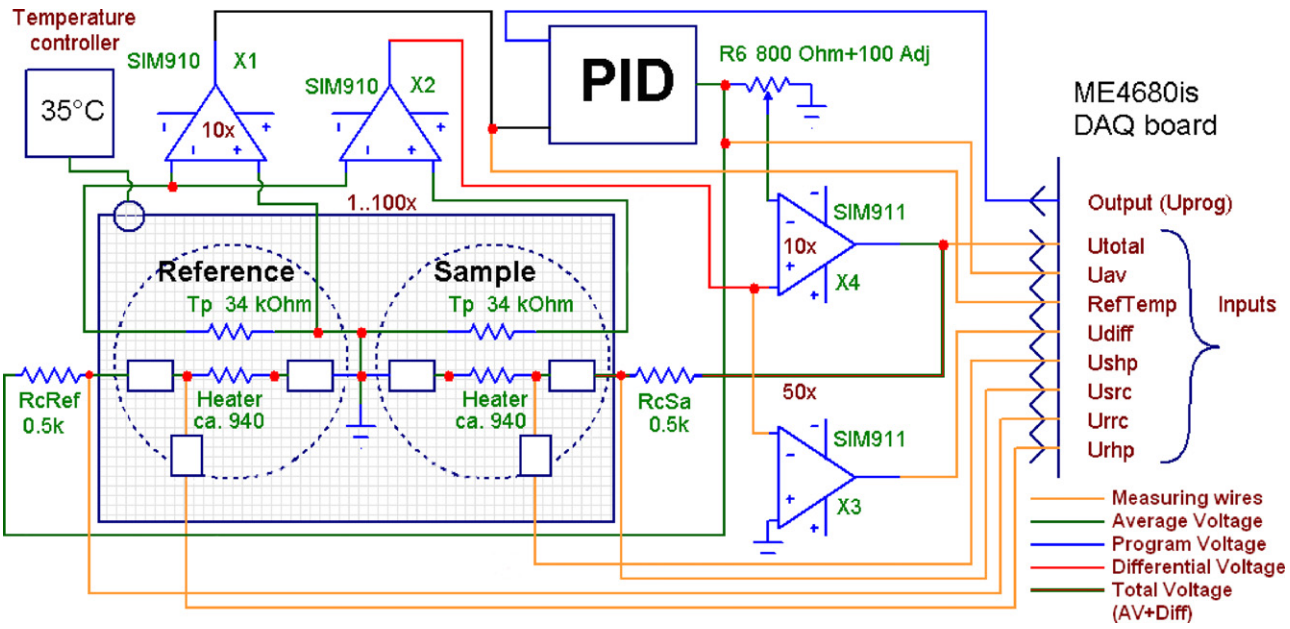

Fig. 4. Scheme of differential fast scanning calorimeter with power compensation. All needed voltages for power difference and sample temperature determination are shown by orange (thin light) wires.

device [9] we know that the maximum power needed to heat a XI-320 sensor loaded with a 20 ng polymer sample at 1000 K/s to 300 K above the ambient temperature is of the order of 40 mW. The power difference $P_{diff}(T)$ we are interested in is only a few ten μW. Even the voltages and resistances needed could be determined from the quantities measured according to Fig. 4, the problem arises that we are looking for a small difference between two large signals. Consequently, the differential signal will be rather noisy. Therefore the direct subtraction of power on both heaters was not used. Instead the small unavoidable remaining temperature difference of the proportional controller, which determines the power difference, was used. For that the sample side voltage can be written as the sum of the differential and the average part

$$U^h_{sample} = (U^h_{sample})_{diff} + (U^h_{sample})_{av} \tag{1.6}$$

where the summing is performed by X4. This yields:

$$P_{diff}(T) = \frac{((U^h_{sample})_{diff} + (U^h_{sample})_{av})^2}{R^h_{sample}} - \frac{(U^h_{ref})^2}{R^h_{ref}}$$

$$P_{diff}(T) = \frac{((U^h_{sample})_{diff})^2}{R^h_{sample}} + \frac{2(U^h_{sample})_{diff}(U^h_{sample})_{av}}{R^h_{sample}} + \left(\frac{((U^h_{sample})_{av})^2}{R^h_{sample}} - \frac{(U^h_{ref})^2}{R^h_{ref}}\right) \tag{1.7}$$

where the last two terms in the bracket are the average powers P_0^{sample} and $P_0{}^{ref}$ provided to sample and reference side by the PID controller, respectively. $P_{assym} = (((U^h_{sample})_{av})^2/R^h_{sample}) - ((U^h_{ref})^2/R^h_{ref})$ describes the asymmetry of power distribution from the PID between both sensors, which mainly depends on the difference in their resistances. To artificially modify P_{assym} the adjustable divider R6 was introduced before the summing amplifier X4. It can be used to correct for large asymmetries between both sensors, e.g. due to a large sample surface area.

To calculate the power difference:

$$P_{diff}(T) = \frac{((U^h_{sample})_{diff})^2}{R^h_{sample}} + \frac{2(U^h_{sample})_{diff}(U^h_{sample})_{av}}{R^h_{sample}} + P_{assym} \tag{1.8}$$

heater voltages and resistances are required to be expressed via probed voltages. For determination of sample heater resistance precise high stable constant resistors (R_{cSa}, R_{cRef}) were used for the electric current measurements. To compensate the unknown wiring resistances (including wires on the sensor membrane) a 3-point probe resistance measurement was used assuming symmetric wiring. Resistance can be expressed via probed voltages as:

$$R^h_{sample} = R_C \frac{2U_{shp} - U_{src}}{U_{total} - U_{src}} \tag{1.9}$$

where R_C is the resistance of constant resistor, U_{shp} is the voltage at sample heater (3rd wire), U_{src} is the voltage drop at constant resistor and U_{total} is the total voltage across sample side (probed at the output of X4).

Knowing the resistance of the heater and all other components of the circuit we can define the ratios between the voltage drops on the heater and the measured signals $(U^h_{sample})_{diff}/U_{diff}$ and $(U^h_{sample})_{av}/(U_{total} - U_{diff})$, where U_{diff} is the differential voltage after amplifier X2 (probed through X3). Introducing

$$\alpha = \frac{2U_{shp} - U_{src}}{U_{total}} \tag{1.10}$$

yields for the heater voltages $(U^h_{sample})_{diff} = \alpha U_{diff}$ and $(U^h_{sample})_{av} = \alpha(U_{total} - U_{diff})$ and with Eq. (1.7):

$$P_{diff}(T) = \alpha^2 \left(\frac{(U_{diff})^2}{R^h_{sample}} + \frac{2U_{diff}(U_{total} - U_{diff})}{R^h_{sample}}\right) + P_{assym} \tag{1.11}$$

This will be later on used for the determination of the heat flow rate into the sample.

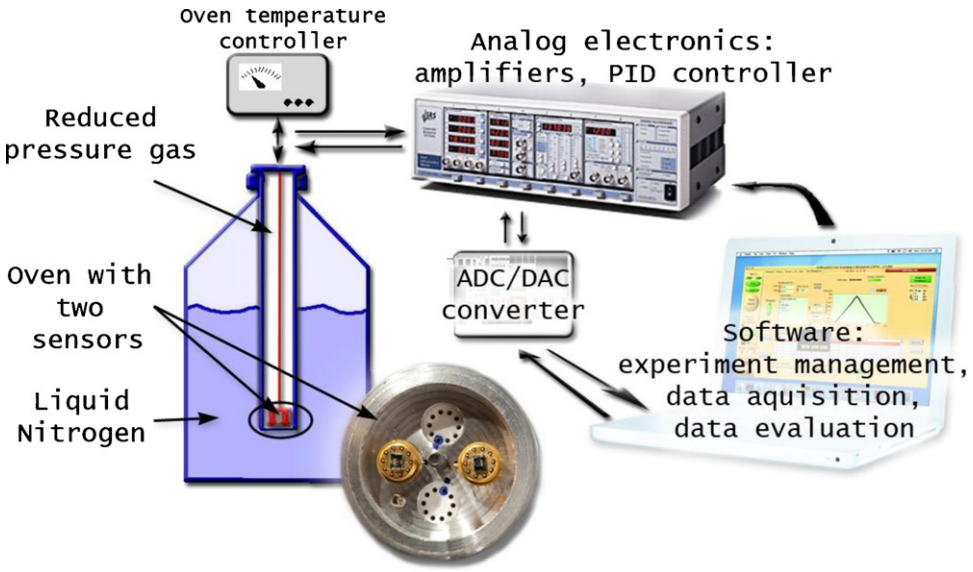

Fig. 5. The fast scanning calorimeter setup. Sensors are placed in an oven at the bottom of a tube in a (reduced pressure) gas environment. Heaters and thermopiles are connected to analog electronic devices. The electronics is driven from a computer by a fast ADC/DAC board (temperature setpoint determination and data collection). The electronic devices are controlled by software which is also used for data collection/evaluation.

4. Hardware and software realization

The setup consists of thermostat, control analog electronics, ADC/DAC converter, computer and software package as schematically shown in Fig. 5.

The cryostat was originally developed for an AC-calorimeter [10] and used for the single sensor fast scanning chip calorimeter [45]. It was further developed for differential AC-chip-calorimeters [46] and adapted for the fast scanning chip calorimeter described here. Both calorimeters, AC and fast scanning, are planned to be integrated and used complementary on the same sample in future.

At the bottom part of the tube is an oven with two chip sensors inside, which is kept at constant controlled temperature. The tube can be pumped and refilled with nitrogen or helium at controlled pressure (preferable 50 kPa [11]). To allow heating of the sample from low temperatures the tube can be placed into liquid nitrogen. Therefore it should be long enough and have thin walls preventing heat transfer in axial direction. This way a very effective, low liquid nitrogen consuming cryostat is realized.

4.1. Electronics

The realization of the above described scheme for scanning rates of several thousand Kelvin per second requires appropriate fast electronics. Therefore it was decided to use analog amplifiers and a PID controller. Stanford Research Systems (SRS) Small Instrumentation Modules (SIM) [44] were used for that. It is a ready-to-use system with adjustable parameters and PC communication interface.

The signals from thermopiles are going to analog amplifiers with high input impedance (100 MΩ, 35 pF) and 1 MHz bandwidth (X1, X2). The amplifier (SIM 910) X1 applied to the reference sensors' thermopile signal is used in single-ended mode. The amplifier X2 is in differential mode amplifying the small temperature difference between sample and reference sensor. Shielding, gain settings and status are controlled remotely from the PC via a serial interface.

The reference temperature amplifier feeds the analog PID controller (SIM 960), which compares the voltage with the setpoint received from the computer. The proportional gain is set to 1 because of the more advanced preamplifier X1. The integral gain is found to be optimal at $10^4\ s^{-1}$ for the used sensors. A bandwidth of 100 kHz, is the limiting factor of this temperature control unit. Larger bandwidth of 1 MHz and smaller noise level has the amplifier (SIM 911) for the proportional power compensation circuit. Same amplifiers were used for thermopile voltage and voltage difference preamplification.

The PID output voltage is applied via limiters and constant resistors to both heaters. These resistors are used not only for current determination but also for avoiding sensor damage by dangerous voltage spikes. For the same reason the power compensation circuit amplification is switched to maximum only during measurements.

The possibility of remote operation is widely used in the control software for the new device. This control is only used for changing parameters of the devices before and after the measurements. Therefore it does not require an extremely fast communication rate. Much faster rates are needed for the temperature setpoint signal and the data acquisition.

4.2. Data aquisition

The Meilhaus DAQ board ME 4680 was chosen for generating and receiving signals [43]. It has an input and output rate of 500,000 s^{-1} (shared between 8 channels), and 16 bit DAC/ADC converter, which make it suitable for the described device.

The output of the board generates the user defined voltage which is used as the setpoint for the PID temperature controller. The ability of generation of an arbitrary "set" of points and direct temperature control gives freedom to the experimentalist in performing non-classical (non-linear) temperature treatments too.

The required voltage data are collected during the experiment by 8 inputs with "Sample&Hold" function. Fast measurements (above 1000 K/s) require fast data acquisition, slow (below 100 K/s) scans should have reduced acquisition rate, avoiding data overflow.

The program voltage profile feed to the PID controller is recalculated from the chosen temperature profile using a thermopile calibration function, which can be chosen from a list depending on sensor and environment [47]. The differential power is recalculated immediately as described above and from that heat capacity is determined, see part 2 [33].

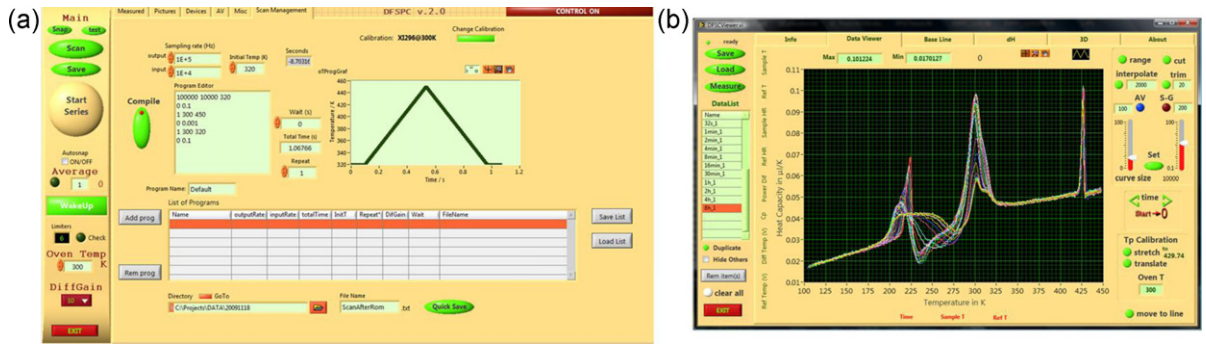

Fig. 6. Screen shot from the software for the fast scanning calorimeter. (a) Part of the temperature profile programming tab. (b) Obtained data after evaluation, including heat capacity determination [33].

4.3. Software

The experiment management software is used for performing one or a series of experiments one by one and saving them, see Fig. 6(a). Saved data contains all input raw voltage data and some recalculated values: reference and sample temperature, reference and sample heating rate and differential power. For easy evaluation and comparison of curves collected by the measurement software and for heat capacity calculation a separate viewer software was developed, see Fig. 6(b). The main idea was a separation of evaluation and acquisition software as well as improvement of performance of each part and possibility of additional functionality without memory overload.

The viewer software includes data manipulation like smoothing, interpolation and fitting of signals specific for this device. It was intended to be the complete FSC data evaluation software which produces final results, including specific heat capacity [33], avoiding the use of additional programs. The experimental results are saved into structured ASCII files which can be imported into any other software. Next, some examples are presented to demonstrate the possibilities and limitations of the new device.

5. Solidification of metals studied by the fast scanning calorimeter

For testing the device melting and crystallization of small spherical metal particles (μm diameters) were studied. For such first

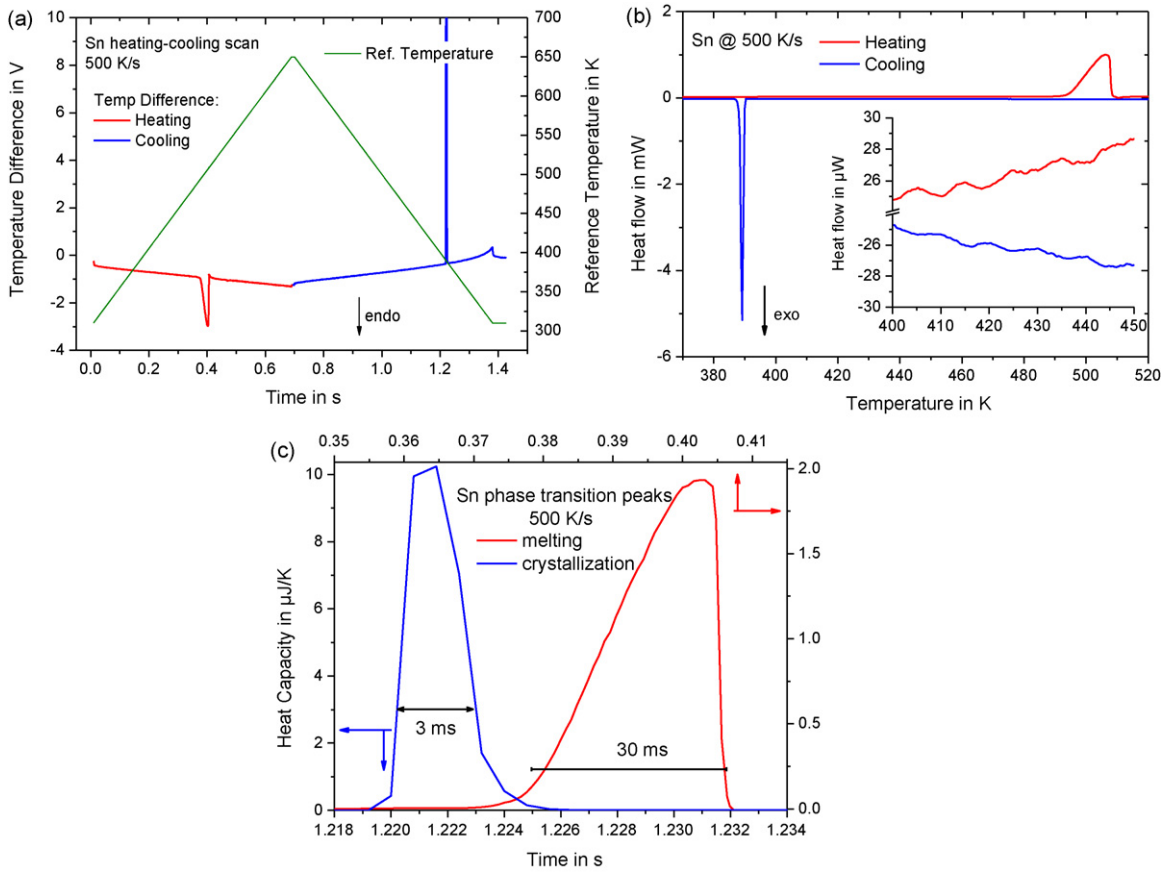

Fig. 7. Heating–cooling of a tin sample of 250 ng at 500 K/s. (a) Remaining temperature difference and temperature profile, (b) recalculated power difference. The inset is a zoomed in part of the curves showing noise of about 1 μW peak-to-peak, which corresponds to about 1 nJ/K and (c) scaled peaks for comparison (be aware of the different scales for heat capacity as well as for time).

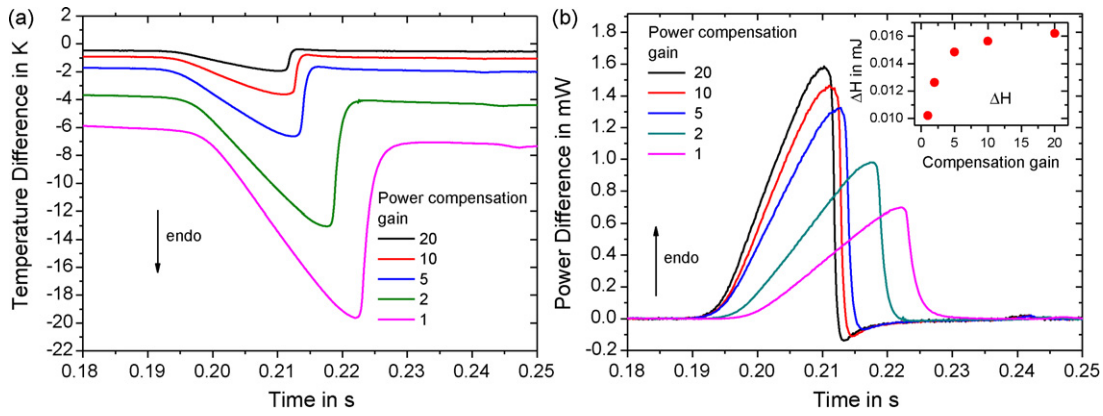

Fig. 8. Influence of differential controller gain setting on the resulting curves for a tin sample of about 250 ng at 1000 K/s heating rate. (a) Remaining temperature difference during the melting transition. (b) Recalculated power difference and heat of fusion (inset), which saturates with higher gain settings indicating that power compensation works properly.

order phase transitions the expected heat capacity and the resulting heat flow curves are known. Even the particles were small the heat of fusion was large compared to the addenda heat capacity of the sensors. Therefore strong deviations of the programmed temperature profile were detected at low differential gain settings as shown below. Nevertheless, at proper gain settings the instrument is capable to handle such transitions in a very good manner.

In order to observe melting and crystallization a Sn particle was heated from room temperature up to 650 K and cooled back at 500 K/s. The temperature profile and the obtained remaining temperature difference are shown in Fig. 7(a). Recalculated heat capacity on heating and cooling are represented in Fig. 7(b and c).

On heating the peak shape is determined by the heat transfer from the sensor to the relatively heavy sample. The expected linear leading edge of the peak is seen in Fig. 7(c). Crystallization on cooling is much faster because of about 100 K supercooling. Therefore heat flow rate during crystallization can be considered as a delta function of about 16 μJ. As shown in Fig. 7(c) the width of the crystallization peak is only 3 ms. The sharp crystallization peak nicely demonstrates the power of the device in handling fast processes also on cooling. The crystallization peak maximum in Fig. 7(b) equals ca. 5 mW. For a 50 ng polymer sample with a heat capacity of about 50 nJ/K this cooling power for the sample alone allows for a cooling rate of about 10^5 K/s. Here we show the reaction time of the device for the sensor XI-320. If one wants to study faster processes one should use sensors with one thermopile and smaller heated area (e.g. XI-292), which is also suited for faster cooling rates.

The effect of differential gain (gain of X4 in Fig. 4) is shown in Fig. 8(a) for a relatively large tin sample of about 250 ng. For low gain settings the melting peak is much broader than for higher gain settings. Not enough heat is given to the sample sensor, and consequently to the sample, allowing the sample to melt as fast as limited by the heat transfer (thermal resistivity) between sensor and sample. Only at high gain settings this limit is reached and a limiting shape of the peak is seen. At low gain settings prerequisites for the power determination described above, like equal temperature for reference and sample sensor, are not fulfilled during melting. Therefore the area, see inset, is smaller and reaches the true value only for gain settings above 10. From the particle diameter of ca 20 μm a sample mass of m_{size} = 250 ng was estimated, which yield a heat of fusion of 17 μJ. The measured heat of fusion (Fig. 8(b)) was 16 μJ. This rough estimation (diameter determination as a main source of error) shows that quantitative determination of heat of fusion is possible.

Fig. 9 shows a comparison of data obtained by the single sensor fast scanning calorimeter without power compensation [11] and the differential fast scanning calorimeter with power compensation. The power compensation yields much sharper peaks, which show the expected shape for a thermal resistivity limited heat flow rate to the melting sample. The estimated enthalpy of fusion from

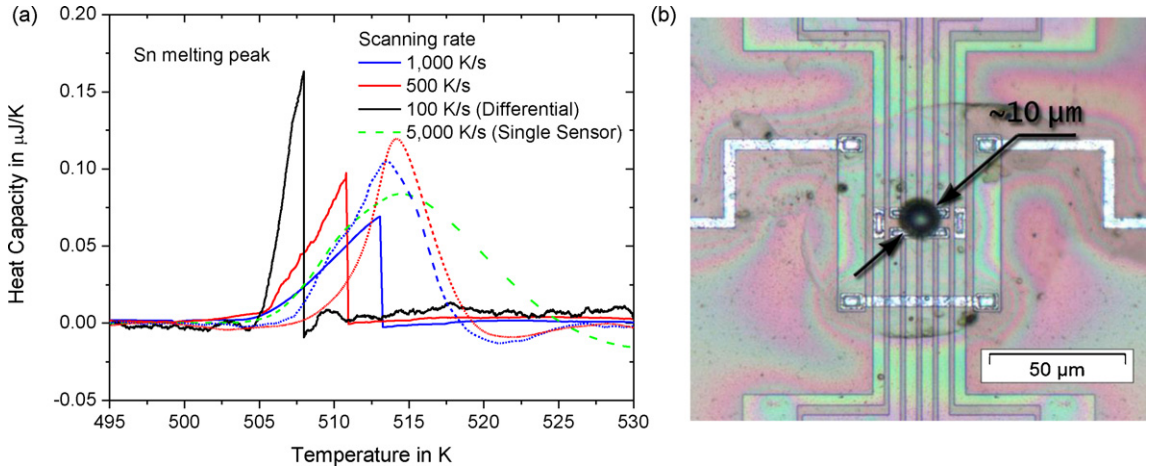

Fig. 9. Heating scans of a 24 ng tin sample at different rates on sensor XI-296. (a) Data from the single sensor device (dashed lines) and the differential setup with power compensation (solid lines) are shown for comparison. (b) The same sample on the same sensor was measured in both devices.

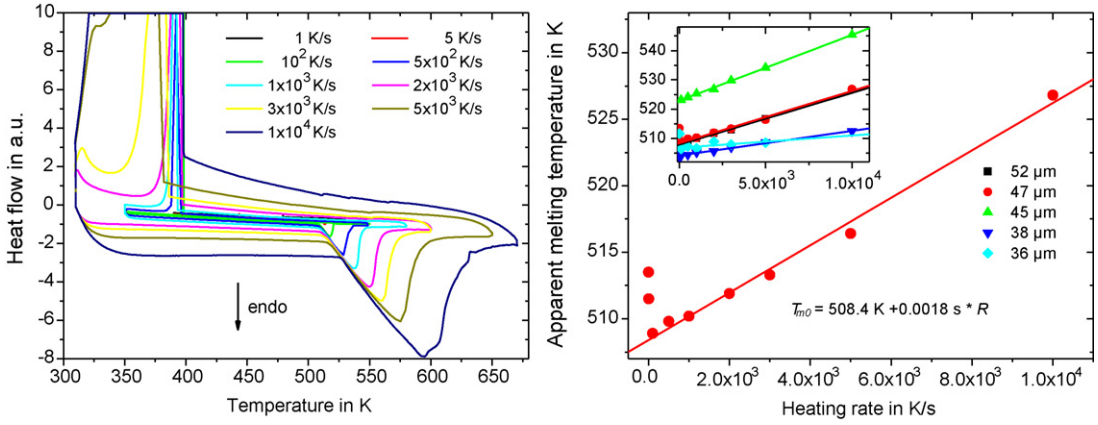

Fig. 10. Metal particle melting and crystallization at different rates. (a) Measured heat flow. (b) Heat transfer correction by melting onset temperature [48].

the size (ca. 10 μm) is 2.5 μJ. The measured value was 2.9 μJ which corresponds to an 11 μm particle.

6. Temperature calibration

The results of similar melting-crystallization scans for another metal particle (SnAgCu alloy) at different heating-cooling rates are shown in Fig. 10(a) [48]. The melting point shifts with increasing heating rate due to the heat transfer problem (thermal lag). This problem is known from conventional DSC too and is commonly solved in the following way [49]: the peak onset temperatures are plotted as function of heating rate. A linear fit function is used to interpolate or extrapolate, e.g. to negative rates (cooling) as needed. Such a calibration measurement is shown in Fig. 10(b) [50]. For some reasons the data points at low rate deviate from the straight line. The origin of this effect could be an additional heat transport mechanism becoming important only at low rates, e.g. convection. At high rates it is assumed that sample and sensor are cooled only by thermal conduction through the gas [12]. To reduce the influence of convection one should make the sample as flat as possible, what was not an option for the measurements of spherical particles [48,51,52]. This undefined additional heat transfer between sample and measuring system, as it is known from two-dimensional heat flux DSCs too [53], limits accuracy of the temperature measurement by the thermopile in the membrane significantly.

To study the influence of a low thermal conductive polymer sample on the temperature measurement a more complex sample was investigated. A first flat indium particle of ca. 18 ng was placed directly on the membrane and a second one of ca. 6 ng on top of a polymer sample, which covers the first indium particle, see Fig. 11. The tiny indium particle on top of the polymer sample was used to study the additional thermal lag due to the polymer sample.

For temperature calibration we follow the procedure for temperature calibration of differential scanning calorimeters (DSC) recommended by GEFTA [49]. Fig. 12 shows the peak onset temperatures of the indium melting peaks as function of heating rate. For the first indium particle, directly placed on the sensor (Fig. 11(a)), the linear behavior is extrapolated to zero heating rate and the obtained value allows calibration of temperature in the common way. Accordingly, the intersect at zero heating rate is shifted to the expected value of 429.9 K. The calibration procedure is performed with at least a second standard considering temperature dependencies of the calibration factors. All calibrations are performed at the same base temperature to simplify thermopile calibration [47].

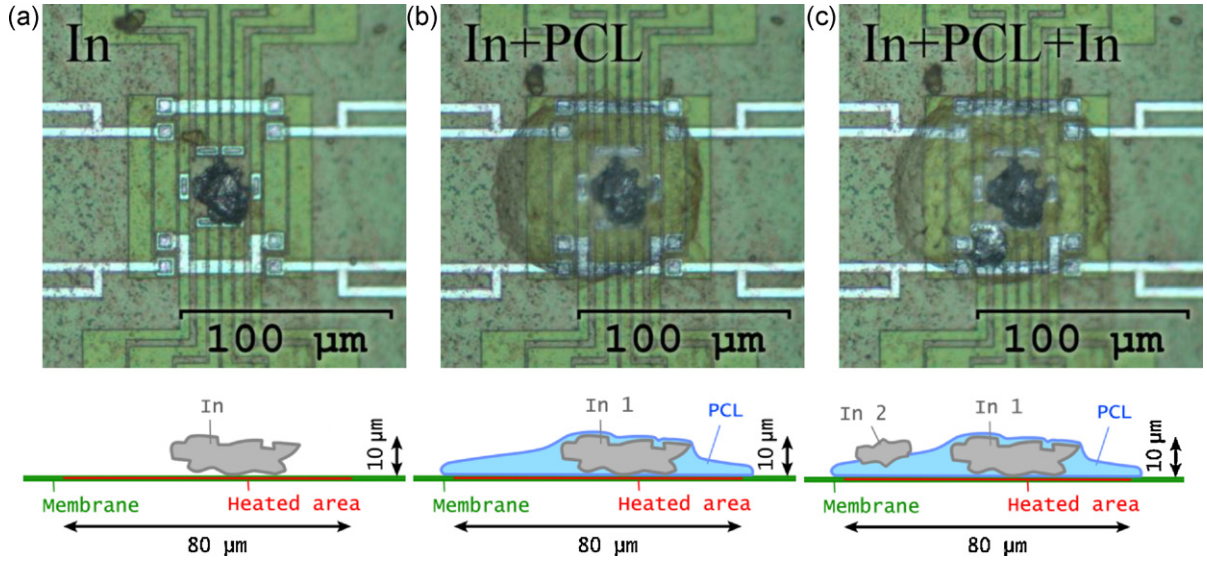

Fig. 11. The three samples measured for temperature calibration purposes on a sensor XI-320. (a) Indium in the center of the empty sensor. (b) The same indium sample covered with poly ε-caprolactone, which was placed as a small particle on the indium and then melted (Aldrich, 55,700 g/mol). (c) The polymer covered sample from (b) with another indium particle on top of the polymer 30 μm away from the center.

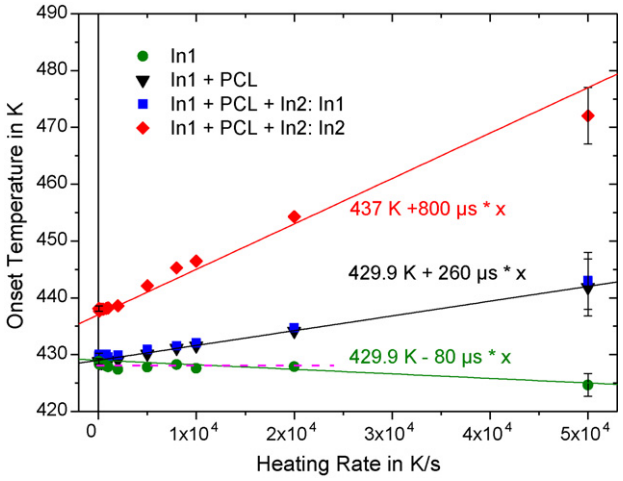

Fig. 12. Melting onset versus heating rate of the two indium particles from Fig. 11. The lowest curve (green dots) corresponds to the first particle as shown in Fig. 11(a). The middle line shows the melting onset of the first particle covered by a polymer (PCL) sample (Fig. 11(b)) (blue squares) and Fig. 11(c) (black triangles). The upper curve corresponds to the second indium particle on top of the polymer, Fig. 11(c) (red diamonds). (For interpretation of the references to color in this figure legend, the reader is referred to the web version of the article.)

As seen from Fig. 12 the thermal lag for the particle on the membrane is practically zero (−80 μs). This unexpected negative slope is related to the different coupling between heater and sample and heater and thermopile, which yields a delayed heating of the thermopile in the membrane compared to the better coupled In sample at the highest rate. For the data up to 2×10^4 K/s a horizontal line (pink dashed curve in Fig. 12) is obtained. This effect is not further considered here because influences discussed below cause much bigger uncertainties.

The second curve from bottom shows the peak onset data for the first indium particle covered by a polymer sample (Fig. 11(b)). Now a thermal lag is observed, which may be caused by the added heat capacity of the polymer on top of the In particle. Furthermore, due to capillary forces a polymer layer can form between the indium sample and the sensor surface, increasing the thermal resistance compared to the very thin gas layer for the In particle alone. The thermal lag becomes 260 μs, which is still a very small value yielding a temperature gradient of less than 3 K at 10^4 K/s. For the second indium particle on top of the polymer sample (Fig. 11(c)) thermal lag reaches 800 μs. This corresponds to a temperature gradient inside the polymer sample of about 8 K at 10^4 K/s. From this curve a rate dependent calibration can be obtained or the sample thickness can be adapted until an acceptable gradient is obtained. While intersects at zero heating rate for all curves of the first particle are the same, the curve for the small second indium particle intersects at a temperature about 8 K higher. Nevertheless, for both particles the line can be extrapolated to negative rates (cooling) for calibration purposes [53,54], assuming a symmetric operation of the device [48], which is justified because even at controlled cooling the heater provides the heat compensating the heat losses and needed to control temperature.

Beside the heat transfer problem (thermal lag) there is an additional problem influencing accuracy of the temperature measurement. Even the heated area is small it is not homogeneously heated for the large sensors used here because the heater consists of two resistive heater stripes, see Figs. 13 and 14. The temperature profile around the heater was investigated by infra-red thermography and analytical modeling of the sensor-gas system [34]. The temperature gradient outside the heated area is very steep and requires a correct placement of the sample in between the two heater stripes. A more detailed analysis of the temperature profile inside the heated area became possible by watching the nematic–isotropic transition of the liquid crystal 8OCB, which was used for temperature calibration purposes in DSC before [53,55], by polarized optical microscopy. The contour lines of the phase transition temperature are seen in Fig. 13. Temperature differences inside the heated area of several Kelvin as well as some asymmetry of the temperature distribution are detected for the sensor XI-296. These data show again how important a proper placement of the sample is. For precise heat capacity determination the placement of the sample inside the heater area is mandatory. If the sample spreads out of the heater area, e.g. for spin coated or otherwise on the sensor deposited films sample temperature is not well defined, even measurements on such samples are possible.

The main issue of metallic particle measurements is the small heat contact area. Especially for spherical particles heat transfer between the sensor and the sample is limited, see Fig. 14. One solution to overcome this problem is to place grease in between sample and membrane. Depending on viscosity and surface tension it can improve heat transfer significantly. One should take care about the stability of the grease in the temperature range of the experiment and about symmetry of the differential system. Furthermore the same amount of grease is placed on the reference sensor to minimize the difference in addenda heat capacity. This one can do by placing a small amount of it on the sensor and performing scans at needed rates. Normally the amount of grease staying in the heater area is less than 1 ng, which is small in comparison to common sample masses above 10 ng. After several heating–cooling scans nearly the same amount of grease will remain on both sensors. The additional asymmetry in addenda heat capacity may be of the order of 0.1 nJ/K, which can be neglected in most cases. Furthermore, it is possible to perform an "empty" sensor heat capacity measurement, which is then subtracted from the sample scan, in analogy to classical DSC. Nevertheless, the particle feels the temperature of the contact spot with the sensor surface and this temperature may be different from that measured by the thermopile. This also explains the vertical shift of the curves for different particles as shown in the inset of Fig. 10(b) and in Fig. 12. For different samples (different thermal contact resistances) lines with different slopes but the same intersect at zero rate are expected. The observation of different intersects is due to different placement of the tiny particles on the sensor, see Fig. 11(c), probing this way the temperature profile as shown in Fig. 13.

The data presented indicate that there are other effects than thermal lag influencing temperature measurement by the thermopile of the chip sensor. One effect is the lateral temperature profile in the heater area. For the sample under investigation it limits accuracy of the temperature measurement to about ±10 K. From the slope of the curve for the indium particle on top of the polymer we see that at 1000 K/s an additional shift of about 1 K and at 10,000 K/s of 8 K has to be considered. While the position of the sample cannot be controlled perfectly the thermal lag effect can be corrected for. The indium particle on top of the sample allows for a temperature calibration taking into account thermal lag and other influences from the sample. Then the accuracy for temperature is ±4 K and reproducibility ±1 K. If temperature measurement depends on a previous calibration uncertainty may reach ±10 K but reproducibility is still within ±1 K. The problems discussed here are not related to bad thermopile or heater resistance temperature calibration, they are mainly caused by the lateral temperature profile in the sensor and its change due to the sample. Therefore sample temperature measurement for these chip calorimeters requires improvement and the data shown above point to different possibilities. (i) The lateral temperature profile should be averaged by a good

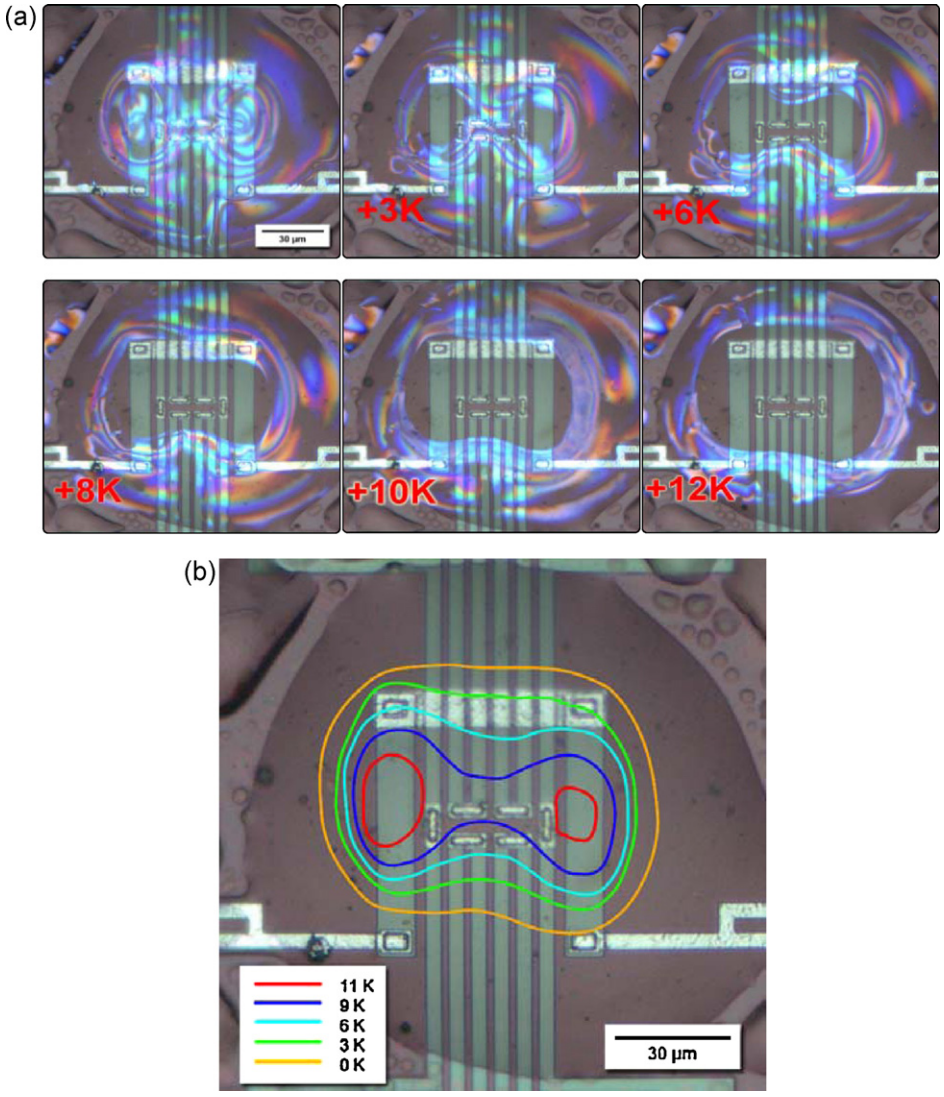

Fig. 13. (a) Temperature profiles of the heated sensor XI-296 probed by the nematic–isotropic transition front of the liquid crystal 8OCB by polarized optical microscopy. (b) Temperature contour lines for different heater powers.

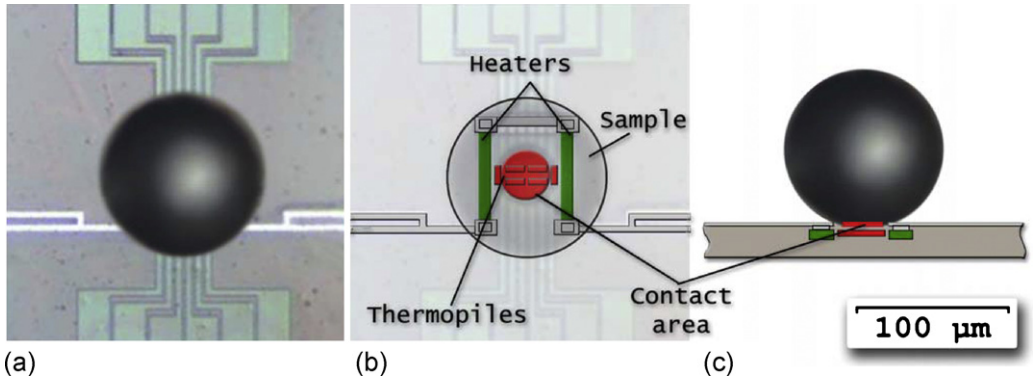

Fig. 14. (a) Spherical particle placement on sensor XI-296 and (b and c) illustration of the contact area problem.

thermal conducting layer, e.g. metal film, covering heater and thermopile. (ii) Sensors with smaller heated are like XI-292 minimize lateral temperature distribution but require smaller samples too. (iii) Sample thickness must be small enough to avoid perpendicular thermal lag at high rates.

7. Summary

A new differential power compensated fast scanning nanocalorimeter on the basis of thin film chip sensors was constructed. The power compensation scheme was slightly modified compared

to the well-known scheme used in the PerkinElmer DSCs. Instead of controlling the average temperature of both sensors the new scheme controls only the temperature of the reference sensor forcing it to follow the programmed time–temperature profile. A PID controller is used here and the output is feed not only to the reference sensor, which temperature is measured, but to the sample sensor too. Any occurring temperature difference between reference and sample sensor is recognized by a second controller. The output of this differential controller is added to the PID output on the sample side alone. Contrary to the PerkinElmer scheme the differential controller does not act on the reference sensor at all. This way the two control loops are fully separated and can be designed according the particular task they have to solve. We use a PID controller for the reference temperature and a very fast proportional controller for the differential loop. For test purposes the device was applied to the study of melting and crystallization of metals. Cooling power is large and response time is short enough to allow investigation of very fast processes on heating and cooling up to 10^5 K/s, as shown in the given examples.

Reliable temperature measurements with an uncertainty of ± 3 K are possible if a tiny indium or other reference material sample is placed on top of a polymer sample. The uncertainties of ± 10 K for measurements without a reference sample on top of the sample under investigation is not acceptable and needs further studies, improvement of sample placement, and smoothing of the lateral temperature profile.

Determination of heat capacity and specific heat capacity out of the available differential power data on fast scanning will be shown in the second part of this paper [33].

Acknowledgements

We acknowledge helpful discussions with Alexander Minakov, Dongshan Zhou and Yu-Lai Gao as well as financial support by a European Union funded Marie Curie EST fellowship (EZ), Humboldt Foundation, Bosch-Foundation and Functional Materials Rostock e.V. (commercial supplier of AC and fast scanning chip calorimeters).

References

[1] M.F.J. Pijpers, V.B.F. Mathot, B. Goderis, R. Scherrenberg, E. van der Vegte, High-speed calorimetry for the analysis of kinetics of vitrification, crystallization and melting of macromolecule, Macromolecules 35 (2002) 3601–3613.
[2] PerkinElmer_Inc., Technical Specifications Thermal Analysis for the DSC 8000/8500 Differential Scanning Calorimeters http://las.perkinelmer.com/content/RelatedMaterials/SpecificationSheets/SPC_8000and8500.pdf (2009).
[3] N.E. Hager, Thin heater calorimeter, Rev. Sci. Instrum. 35 (1964) 618–624.
[4] L.H. Allen, G. Ramanath, S.L. Lai, Z. Ma, S. Lee, D.D.J. Allman, K.P. Fuchs, 1,000,000 °C/s thin film electrical heater: in situ resistivity measurements of Al and Ti/Si thin films during ultra rapid thermal annealing, Appl. Phys. Lett. 64 (1994) 417–419.
[5] M.Y. Efremov, E.A. Olson, M. Zhang, F. Schiettekatte, Z. Zhang, L.H. Allen, Ultrasensitive, fast, thin-film differential scanning calorimeter, Rev. Sci. Instrum. 75 (2004) 179–191.
[6] M. Chonde, M. Brindza, V. Sadtchenkoa, Glass transition in pure and doped amorphous solid water: an ultrafast microcalorimetry study, J. Chem. Phys. 125 (2006).
[7] E. León-Gutierrez, G. Garcia, M.T. Clavaguera-Mora, J. Rodríguez-Viejo, Glass transition in vapor deposited thin films of toluene, Thermochim. Acta 492 (2009) 51–54.
[8] A.F. Lopeandía, J. Rodríguez-Viejo, Size-dependent melting and supercooling of Ge nanoparticles embedded in a SiO_2 thin film, Thermochim. Acta 461 (2007) 82–87.
[9] S.A. Adamovsky, A.A. Minakov, C. Schick, Scanning microcalorimetry at high cooling rate, Thermochim. Acta 403 (2003) 55–63.
[10] A.A. Minakov, S.A. Adamovsky, C. Schick, Non adiabatic thin-film (chip) nanocalorimetry, Thermochim. Acta 432 (2005) 177–185.
[11] A.A. Minakov, C. Schick, Ultrafast thermal processing and nanocalorimetry at heating and cooling rates up to 1 MK/s, Rev. Sci. Instrum. 78 (2007) 073902–073910.
[12] A.A. Minakov, A.W. van Herwaarden, W. Wien, A. Wurm, C. Schick, Advanced nonadiabatic ultrafast nanocalorimetry and superheating phenomenon in linear polymers, Thermochim. Acta 461 (2007) 96–106.
[13] A.W. van Herwaarden, Overview of calorimeter chips for various applications, Thermochim. Acta 432 (2005) 192–201.
[14] A.A. Minakov, D.A. Mordvintsev, C. Schick, Melting and reorganization of poly(ethylene terephthalate) on fast heating (1000 K/s), Polymer 45 (2004) 3755–3763.
[15] A.A. Minakov, D.A. Mordvintsev, C. Schick, Isothermal reorganization of poly(ethylene terephthalate) revealed by fast calorimetry (1000 K s^{-1}; 5 ms), Faraday Discuss. 128 (2005) 261–270.
[16] A.A. Minakov, D.A. Mordvintsev, R. Tol, C. Schick, Melting and reorganization of the crystalline fraction and relaxation of the rigid amorphous fraction of isotactic polystyrene on fast heating (30,000 K/min), Thermochim. Acta 442 (2006) 25–30.
[17] A. Gradys, P. Sajkiewicz, A.A. Minakov, S. Adamovsky, C. Schick, T. Hashimoto, K. Saijo, Crystallization of polypropylene at various cooling rates, Mater. Sci. Eng. A 413–414 (2005) 442–446.
[18] A. Gradys, P. Sajkiewicz, S. Adamovsky, A. Minakov, C. Schick, Crystallization of poly(vinylidene fluoride) during ultra-fast cooling, Thermochim. Acta 461 (2007) 153–157.
[19] F. De Santis, S. Adamovsky, G. Titomanlio, C. Schick, Scanning nanocalorimetry at high cooling rate of isotactic polypropylene, Macromolecules 39 (2006) 2562–2567.
[20] F. De Santis, S. Adamovsky, G. Titomanlio, C. Schick, Isothermal nanocalorimetry of isotactic polypropylene, Macromolecules 40 (2007) 9026–9031.
[21] V.V. Ray, A.K. Banthia, C. Schick, Fast isothermal calorimetry of modified polypropylene clay nanocomposites, Polymer 48 (2007) 2404–2414.
[22] A. Krumme, A. Lehtinen, S. Adamovsky, C. Schick, J. Roots, A. Viikna, Crystallization behavior of some unimodal and bimodal linear low-density polyethylenes at moderate and high supercooling, J. Polym. Sci. Part B: Polym. Phys. 46 (2008) 1577–1588.
[23] C. Silvestre, S. Cimmino, D. Duraccio, C. Schick, Isothermal crystallization of isotactic poly(propylene) studied by superfast calorimetry, Macromol. Rapid Commun. 28 (2007) 875–881.
[24] C. Schick, Differential scanning calorimetry (DSC) of semicrystalline polymers, Anal. Bioanal. Chem. (2009) 1589–1611.
[25] M. Pyda, E. Nowak-Pyda, J. Heeg, H. Huth, A.A. Minakov, M.L. Di Lorenzo, C. Schick, B. Wunderlich, Melting and crystallization of poly(butylene terephthalate) by temperature-modulated and superfast calorimetry, J. Polym. Sci., Part B: Polym. Phys. 44 (2006) 1364–1377.
[26] R.T. Tol, A.A. Minakov, S.A. Adamovsky, V.B.F. Mathot, C. Schick, Metastability of polymer crystallites formed at low temperature studied by Ultra fast calorimetry* Polyamide 6 confined in sub-micrometer droplets vs bulk PA6, Polymer 47 (2006) 2172–2178.
[27] A. Minakov, A. Wurm, C. Schick, Superheating in linear polymers studied by ultrafast nanocalorimetry, Eur. Phys. J. E Soft Matter 23 (2007) 43–53.
[28] V. Brucato, S. Piccarolo, V. La Carrubba, An experimental methodology to study polymer crystallization under processing conditions. The influence of high cooling rates, Chem. Eng. Sci. 57 (2002) 4129–4143.
[29] H. Janeschitz-Kriegl, Crystallization Modalities in Polymer Melt Processing, Fundamental Aspects of Structure Formation, Springer, Wien, New York, 2010.
[30] W. Chen, D. Zhou, G. Xue, C. Schick, Chip calorimetry for fast cooling and thin films: a review, Front. Chem. Chin. 4 (2009) 229–248.
[31] S. Adamovsky, C. Schick, Ultra-fast isothermal calorimetry using thin film sensors, Thermochim. Acta 415 (2004) 1–7.
[32] M.Y. Efremov, E.A. Olson, M. Zhang, S.L. Lai, F. Schiettekatte, Z.S. Zhang, L.H. Allen, Thin-film differential scanning nanocalorimetry: heat capacity analysis, Thermochim. Acta 412 (2004) 13–23.
[33] E. Zhuravlev, C. Schick, Fast scanning power compensated differential scanning nano-calorimeter: 2. Heat capacity analysis, Thermochim. Acta this issue 505 (2010) 14–21.
[34] A. Minakov, J. Morikawa, T. Hashimoto, H. Huth, C. Schick, Temperature distribution in a thin-film chip utilized for advanced nanocalorimetry, Meas. Sci. Technol. 17 (2006) 199–207.
[35] A.F. Lopeandia, J. Valenzuela, J. Rodríguez-Viejo, Power compensated thin film calorimetry at fast heating rates, Sens. Actuators A: Phys. 143 (2008) 256–264.
[36] A.F. Lopeandia, L.I. Cerdo, M.T. Clavaguera-Mora, L.R. Arana, K.F. Jensen, F.J. Munoz, J. Rodríguez-Viejo, Sensitive power compensated scanning calorimeter for analysis of phase transformations in small samples, Rev. Sci. Instrum. 76 (2005) 065104–065105.
[37] M. Merzlyakov, Method of rapid (100,000 K/s) controlled cooling and heating of thin samples, Thermochim. Acta 442 (2006) 52–60.
[38] M.J. O'Neill, The analysis of a temperature-controlled scanning calorimeter, Anal. Chem. 36 (1964) 1238–1245.
[39] M.J. O'Neill, Measurement of specific heat functions by differential scanning calorimetry, Anal. Chem. 38 (1966) 1331–1336.
[40] E.S. Watson, M.O. O'Neill, J. Justin, N. Brenner, A differential scanning calorimeter for quantitative differential thermal analysis, Anal. Chem. 36 (1964) 1233–1238.
[41] E.S. Watson, M.J. O'Neill, Differential Microcalorimeter, The Perskin-Elmer Corporation, Norwalk, CN, 1966.
[42] E. Zhuravlev, C. Schick, Patent pending, USA, 2009.
[43] Meilhaus ADC/DAC board, 2009. http://www.meilhaus.de/fileadmin/upload/download/products/manuals/ME-4600%202.0E.pdf.

[44] SRS Small Instrumentation Module, 2009. http://www.thinksrs.com/products/SIM.htm.
[45] A.A. Minakov, S.A. Adamovsky, C. Schick, Advanced two-channel AC calorimeter for simultaneous measurements of complex heat capacity and complex thermal conductivity, Thermochim. Acta 403 (2003) 89–103.
[46] H. Huth, A. Minakov, C. Schick, High sensitive differential AC-chip calorimeter for nanogram samples, Netsu Sokutei 32 (2005) 70–76.
[47] V.A. Drebushchak, Universality of the emf of thermocouples, Thermochim. Acta 496 (2009) 50–53.
[48] Y.L. Gao, E. Zhuravlev, C.D. Zou, B. Yang, Q.J. Zhai, C. Schick, Calorimetric measurements of undercooling in single micron sized SnAgCu particles in a wide range of cooling rates, Thermochim. Acta 482 (2009) 1–7.
[49] G.W.H. Hohne, H.K. Cammenga, W. Eysel, E. Gmelin, W. Hemminger, The temperature calibration of scanning calorimeters, Thermochim. Acta 160 (1990) 1–12.
[50] S.M. Sarge, W. Hemminger, E. Gmelin, G.W.H. Hohne, H.K. Cammenga, W. Eysel, Metrologically based procedures for the temperature, heat and heat flow rate calibration of DSC, J. Therm. Anal. 49 (1997) 1125–1134.
[51] G. YuLai, Z. ChangDong, Y. Bin, Z. QiJie, Fast calorimetric scanning of micro-sized SnAgCu single droplet at a high cooling rate, Sci. China Ser. E-Technol. Sci. 52 (2009) 1707–1711.
[52] B. Yang, Y.L. Gao, C.D. Zou, Q.J. Zhai, E. Zhuravlev, C. Schick, Repeated nucleation in an undercooled tin droplet by fast scanning calorimetry, Mater. Lett. 63 (2009) 2476–2478.
[53] S. Neuenfeld, C. Schick, Verifying the symmetry of differential scanning calorimeters concerning heating and cooling using liquid crystal secondary temperature standards, Thermochim. Acta 446 (2006) 55–65.
[54] S.M. Sarge, G.W.H. Hohne, H.K. Cammenga, W. Eysel, E. Gmelin, Temperature, heat and heat flow rate calibration of scanning calorimeters in the cooling mode, Thermochim. Acta 361 (2000) 1–20.
[55] C. Schick, U. Jonsson, T. Vassilev, A. Minakov, J. Schawe, R. Scherrenberg, D. Lörinczy, Applicability of 8OCB for temperature calibration of temperature modulated calorimeters, Thermochim. Acta 347 (2000) 53–61.